Structure and spectroscopic properties of oxygen divacancy in yttrium-stabilized zirconia

2008 J. Phys.: Conf. Ser. 117 012022

(http://iopscience.iop.org/1742-6596/117/1/012022)

Journal of Physics: Conference Series **117** (2008) 012022 doi:10.1088/1742-6596/117/1/012022

Structure and spectroscopic properties of Oxygen divacancy in yttrium-stabilized zirconia

D Muñoz Ramo and A L Shluger

Department of Physics and Astronomy and the London Centre for Nanotechnology, University College London, Gower Street, London WC1E 6BT, UK

E-mail: d.ramo@ucl.ac.uk

Abstract. We have studied the structure and spectroscopic properties of the oxygen divacancy defect in Yttrium-stabilized ZrO_2 using periodic and embedded cluster methods and GGA and B3LYP density functionals. The results demonstrate that the defect spectroscopic properties depend on the particular arrangement of Y dopants near vacancies. The optical transition energies calculated for the negatively charged state of the divacancy at 2.8 eV and 3.3 eV are in agreement with experimental data. The second set of transitions between 1.9 eV and 2.7 eV corresponds to the electron transfer between vacancies. The calculated EPR g-tensor values are in agreement with other works. The results support the proposed attribution of the optical absorption peaking at 3.3 eV and related EPR spectra to Zr^{3+} ions in the YSZ matrix, however, they are not fully conclusive due to dependence on Y concentration.

1. Introduction

Zirconia (ZrO_2) is being studied extensively due to its interesting fundamental properties and important applications in solid oxide fuel cells, oxygen sensors and high-temperature coatings, among others [1, 2, 3]. It has three different polymorphs, depending on temperature and pressure. The monoclinic phase is stable in a wide range of temperatures at atmospheric pressure and evolves into the tetragonal phase above 1443 K. Cubic phase is stable above 2643 K and the material melts at 2979 K. Doping with aliovalent cations (such as Ca or Y at 7 to 20 mole % doping) compensated by anion vacancies induces stabilization of the cubic phase at room temperature. In this work we focus on the properties of the most widely used Yttrium-stabilized cubic zirconia (YSZ).

Professor C. Pisani and co-workers [4, 5] were among the first to use periodic *ab initio* methods for investigating the electronic structure of zirconia and transition between the tetragonal and cubic phases as well as hydroxylation of ZrO_2 surfaces. Further *ab initio* studies focused on doped phases, with special attention to YSZ. Some of these studies aimed at elucidating the role of dopants and oxygen vacancies in the stabilization of the cubic phase and its properties [6]. Other theoretical studies tried to relate the presence of these specie in the matrix of ZrO_2 to the spectroscopic data available for this compound. In particular, the identity of the so-called T center, detected in optical absorption and EPR measurements [7, 8], remained controversial for years, being assigned either to a specific divacancy complex or to the presence of Ti impurities [9, 10, 11]. The *ab initio* calculations addressing these issues performed using a periodic model and the Hartree-Fock and Density Functional Theory (DFT) provided accurate information

regarding the electronic structure and EPR g-tensor of YSZ [11]. However, the optical absorption energies have been approximated by one-electron energy differences.

More accurate predictions of spectroscopic properties of this complex system can be obtained through the use of state-of-the-art quantum chemical methods and embedded cluster models (see, for example, Refs. [12, 13, 14, 15, 16, 17, 18]). Several types of embedded cluster techniques have been used successfully to study the structure and properties of defects in ionic oxides, such as MgO (see, for example, [19, 20, 21, 22, 23, 24]), CaO [25] and SiO_2 [26, 27]. In this paper we use an embedded cluster model to study defects in YSZ and calculate their spectroscopic properties. First, we analyze the electronic structure of YSZ using both the embedded cluster method and periodic calculations and then investigate the spectroscopic properties of a divacancy defect. We consider a relatively lightly doped phase of YSZ (only 6.25 % of Y_2O_3 in the structure), which is the first step to a more extended study of effects of different amounts of doping on the electronic and spectroscopic properties of the YSZ system.

2. Crystal structure and computational methods

2.1. Structure of YSZ

First, we need to construct a model of YSZ structure. We started from a 96-atom cubic supercell of c-ZrO_2, with the lattice parameter of 10.17 Å, and substituted four Zr atoms by Y ions and two oxygen atoms by vacancies to compensate the charge mismatch induced by the Y atoms. The distribution of vacancies and yttrium atoms was designed to match a series of constraints obtained in the previous *ab initio* calculations [6]. First, the two vacancies are aligned along the <111> direction and share a Zr atom (bridging Zr atom); second, the vacancies are located in the next-nearest neighbour positions with respect to yttrium. This structure ensures that the phase is stable.

We constructed several arrangements of vacancies and yttrium atoms following these rules, and for each of them optimized the structure by means of classical calculations using Buckingham inter-atomic potentials and the shell model. We chose a classical model to avoid the high computational cost of using periodic *ab initio* calculations for optimizing the structure of these large periodic cells. The potentials, initially developed for cubic ZrO_2 [28] and Y_2O_3 [29], have been modified to make them compatible (see parameters in table 1). These potentials are designed for formal charges on the atoms. The charge on oxygen is distributed between a core (+2.0 e) and a shell (-4.0 e), with a spring constant connecting the core and the shell having the value $k = 200.1$ eV/Å. We obtained several stable supercells with different distributions of Y atoms around the divacancy complex, with energy differences between different cells ranging between 0.1 eV and 0.3 eV. This small energy difference suggests that several Y distributions can coexist at this level of doping of YSZ. The lowest energies correspond to divacancy configurations in which two Y ions share one O site and two other Y ions are located far away from them. Configurations in which more than two Y ions are clustered have higher energies. From these calculations the supercell with the lowest energy was chosen as the starting point for our *ab initio* calculations. The structure of this supercell is shown in Figure 2.1. It is important to note that O vacancies in this model are not equivalent: one of the vacancies is surrounded by four Yttrium ions, while the other vacancy has only three Yttrium ions in its vicinity.

2.2. Methods of calculations

In this study we used both periodic and embedded cluster models. The periodic model allows us to accurately analyze the electronic structure of the system and provides calibration for the embedded cluster model, which is then used for calculating defect spectroscopic properties. Periodic calculations were carried out using two density functionals and basis sets in order to compare their accuracy in the description of the YSZ system. GGA calculation with a plane wave basis set and 500 eV cutoff were carried out using the VASP code [30]. The calculations

Table 1. Values of the parameters of the short-range Buckingham type interatomic potentials between ions in YSZ. A and ρ are the pre-exponential factor and the exponent, and C is the coefficient in the dispersion term, respectively. Only Coulomb repulsion is included between the Zr and Y ions and between the O ions.

pair	A (eV)	ρ (Å)	C (eV Å ^{6})
Zr-O	1610.28	0.34	0.0
Y-O	1618.13	0.320217	26.6911

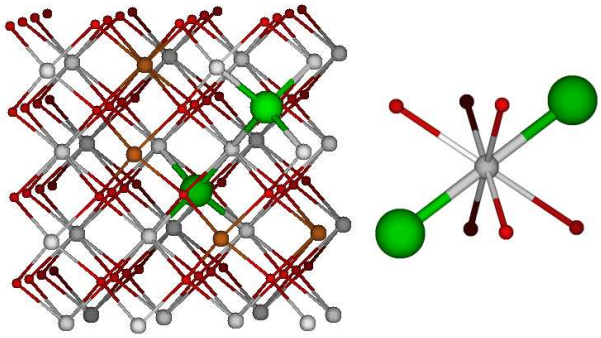

Figure 1. (left) The supercell used as a building block of the YSZ nanocluster. Red balls represent O, white balls - Zr, brown balls - Y, and large green balls are positions of vacancies. (right) Detail of the divacancy complex.

using the hybrid B3LYP functional were carried out using the CRYSTAL06 package [31]. These calculations employ the Gaussian-type basis set on oxygen atoms from Ref. [32]. It includes 14s, 6p, and 1d primitive Gaussians contracted to 1s, 3sp, and 1d shells using a (8/411/1) scheme and has been used in a large number of previous studies of oxides [32]. The standard LANL2DZ basis sets and the corresponding effective core pseudopotentials have been used for Zr and Y atoms. Each of these basis sets consists of 6s, 6p and 4d primitive Gaussians contracted to 3sp and 2d shells using a (411/31) scheme. Eight k-points were used in both calculations. A neutralizing charge background method was used in calculations of charged systems.

In the embedded cluster model, a cluster including a defect is treated quantum mechanically (quantum cluster (QM)) and is embedded into the lattice of classical polarizable ions. The region directly adjacent to the cluster border requires special attention in order to describe correctly the behaviour of the electrons confined inside the QM cluster. Several techniques of different complexity have been suggested (see, for example, [19, 20, 21, 22, 23, 24]) none of which is completely satisfactory. For ionic systems, such as NaCl, MgO, CaO, using effective core pseudopotentials on cations surrounding the QM cluster usually provides reliable results [24, 25]. For ionic-covalent systems, such as SiO_2, more elaborate schemes have been suggested [26, 27]. No scheme developed so far is universal and equally applicable to materials with different type of bonding. In this work we are testing the applicability of the simple method used for ionic systems [24], where the Zr ions surrounding the QM cluster are described by their full ion pseudopotentials. More computational details are given below.

In our calculations the whole system is represented by a spherical nanocluster of 20 Å radius with the QM cluster at its centre. The nanocluster was constructed using as a building block the 94-atom supercell optimized by means of classical calculations as described above. The size and shape of the nanocluster are chosen in such a way as to represent correctly the bulk crystal electrostatic potential inside the QM cluster and the surrounding region and to avoid introducing internal electric field due to dipole or higher multipole moments in the nanocluster. Once the nanocluster was defined for each system, we applied the embedded cluster scheme implemented

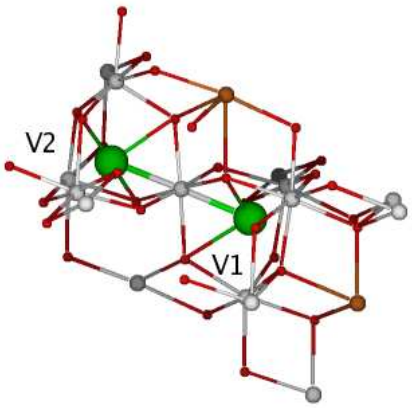

Figure 2. Structure of the QM region in the YSZ embedded cluster model. Red balls are oxygen, white balls are Zr, brown balls are Y, and large green balls mark positions of V_1 and V_2 vacancy cavities.

in the GUESS code [24]. All atoms of the nanocluster are divided into three regions: a QM cluster (see Fig. 2.2), a classical polarizable region (region I), and the rest of the atoms belong to a classical nonpolarizable region II. The QM cluster is composed of 49 atoms, including 32 O, 15 Zr and two Y atoms and has the total charge of +2e. The classical polarizable region I has the radius of 10 Å to ensure correct description of the defect-induced lattice relaxation. The rest of the nanocluster is represented by classical, non-polarizable ions.

Ions in region I are treated using the classical shell model and inter-atomic potentials presented in Table 1, which account both for the Coulomb and the short-range interactions between classical shells. To prevent an artificial spreading of electronic states outside the quantum cluster, all Zr and Y ions in the radius of 10 Å from the center of the nanocluster are described by their effective-core potentials. The interaction between these centers and the quantum oxygen atoms should be adjusted to provide a seamless transition between the two regions and avoid causing lattice distortion by the boundary. For that purpose, we developed a set of correcting potentials of the form:

$$V_c = C_1(r - r_0)^2 + C_2(r - r_0)^3 + C_3(r - r_0)^4 + C_4(r - r_0)^5$$

The parameters for these potentials are specified in Table 2.

Table 2. Values of the parameters of correcting potential for the cation ECP – quantum oxygen interaction.

pair	R_0 (Å)	C_1 (eV/Å^2)	C_2 (eV/Å^3)	C_3 (eV/Å^4)	C_4 (eV/Å^5)
Zr–O	1.5462	19.8062	-29.1185	15.1105	-2.666
Y–O	2.3344	7.0784	-6.6129	2.5671	0.0

The positions of all centres in the QM and classical polarizable regions are fully optimized in the course of the energy minimization, while those in the rest of the nanocluster are kept fixed in the perfect lattice sites.

Quantum mechanical calculations in the embedded cluster model were performed with the GAUSSIAN03 package [33]. We have used the same localized Gaussian basis sets on O, Zr and Y ions and the hybrid B3LYP functional as in the periodic CRYSTAL calculation. Optical transitions were calculated using the time-dependent density functional theory (TD-DFT) method implemented in GAUSSIAN03, and the g-tensor calculations were also performed with the routines implemented in this package.

3. Results and discussion

Two charge states of the divacancy in YSZ have been studied: one corresponding to the neutral system and the other to the negatively charged system. For convenience, we will call the position of the first vacancy V_1 and the position of the second vacancy V_2 (see Fig. 2.2 for reference). The lattice distortion obtained for the neutral state of the system by all three methods used in this work is similar to that observed for the V^{2+} vacancy in pure ZrO_2 or HfO_2 [34]. Specifically, the NN-cations displace away from the vacancy site by about 0.2 Å, while the NNN-anions move towards it by about 0.3 Å. In the divacancy, the bridging Zr ion is shared between V_1 and V_2. The repulsion induced by one of the vacancies on this ion is compensated by the repulsion induced by the other vacancy, and the distance of this Zr ion from each of the vacant sites is significantly shorter than the other Zr-V distances and similar to the Zr-O distance in perfect cubic ZrO_2.

The value of the band gap depends on the method used. In GGA, the gap is about 4.0 eV, while in the periodic B3LYP calculations the gap increases to about 5.8 eV, and in the embedded cluster model the value of 6.3 eV is obtained. Comparison of the density of states between periodic and cluster models shows good agreement of the general features: the valence band is composed of Oxygen p states with a small contribution of Zr p states. The lower part of the conduction band is composed of Zr d states with a small admixture of the Oxygen p states. The yttrium states are present below 20 eV from the top of the VB and at 5.4 eV and higher above the CBM. This means that the nature of the gap region in this model of YSZ is similar to that in pure, undoped cubic ZrO_2.

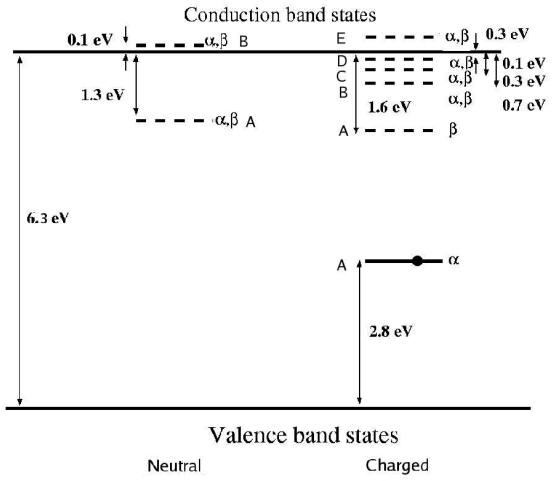

Figure 3. One-electron defect level diagram for the oxygen divacancy in YSZ, calculated through the embedded cluster model. Continuous lines refer to occupied levels, while dotted lines correspond to unoccupied levels. α and β symbols mark spin of the state. Localized levels are labeled with the letters A, B, C, and D.

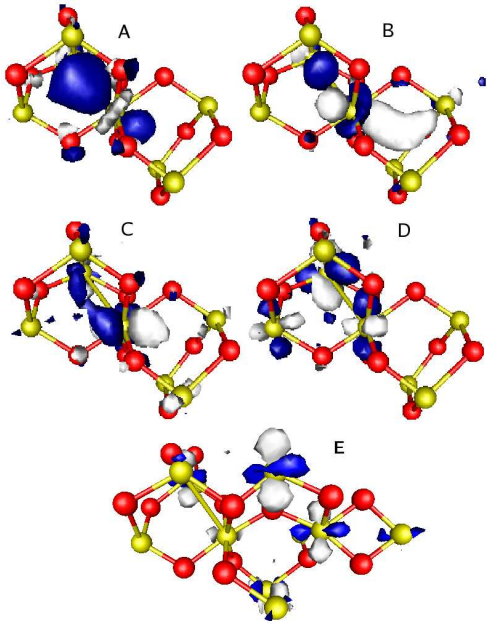

Figure 4. Isosurface representation (value=0.047) of the localized states induced by the oxygen divacancy in YSZ. Zr atoms are represented by dark balls, while O atoms are represented by light balls. A, B, C, and D labels correspond to the localized states shown in Figure 3

The perturbation induced by the divacancy produces two localized states in the gap in the

one-electron spectrum. The exact position of these states in the gap varies with the method used. Figure 3 shows positions of the levels obtained in the embedded cluster calculation. The nature of these states is illustrated in Figure 4. The lowest energy state, labelled A in Fig. 4, is located 1.3 eV below the CBM. Its wavefunction is formed mainly by the linear combination of *d* states of the NN-Zr ions surrounding the V_2 vacancy and has an approximately spherical symmetry. The contribution of the bridging Zr atom to this state is larger than the contributions of other Zr centers. The splitting of this state from the CBM is by about 0.5 eV smaller in the periodic B3LYP calculation and by about 0.2 eV in the GGA calculation. The second state, labelled B in Fig. 4, is located at 0.1 eV above the CBM. The wavefunction of this state is delocalized by both vacancies but there is larger contribution of states corresponding to Zr and O centers surrounding V_1.

The apparent asymmetry of states A and B may be caused by different reasons. In particular, V_1 is surrounded by a slightly larger number of quantum mechanical atoms than V_2. However, comparison with periodic calculations shows that the asymmetry in one-electron states is present in both approaches. A more plausible explanation concerns the distribution of yttrium atoms around the divacancy complex: four Y ions are located close to V_1 and only three Y ions in the neighbourhood of the V_2 cage. Since Y ions are effectively negatively charged with respect to the lattice, this may affect the electron distribution inside the divacancy (*vide infra*).

Natural population analysis (NPA) in this model shows that the presence of the divacancy affects the charge distribution on the ions of the cluster. The O ions NNN to the vacancies have smaller NPA charges, of the order of -1.2 to -1.4 e, while other O ions have charges between -1.5 and -1.9 e. The NN-Zr ions possess charges in the range +2.7 to +3.0 e, except for the case of the bridging Zr ion, which has a charge of +2.3 e. Other Zr ions have effective charges between +3.2 and +3.5 e. The Y atoms in the cluster have NPA charges of +2.6 and +2.8 e, which are very close to the formal charge value of +3.0 e.

Next, we have studied what will happen if an extra electron is added to the system using the same three methods. We found no electron trapping in the GGA calculation, the extra electron is delocalized by Zr ions of the periodic cell. However, both periodic and embedded cluster, B3LYP calculations predict the electron trapping by the divacancy complex. In this case, the lattice relaxation around the cavities changes in response to the new charge state of the divacancy. While the lattice distortion around the V_1 cavity is very similar to the one in the neutral system, the distortion around the V_2 cavity is much bigger. The bridging Zr atom is displaced towards V_2 by approximately 0.1 Å and the V_2-NN-Zr distances are reduced, two of them by approximately 0.05 Å and the third one by about 0.1 Å}. The value of the band gap remains unaffected, but four localized states are induced in the band gap and a resonant state is created above the CBM. The lowest of these states is an occupied state in the α-spin 2.8 eV above the VBM. The corresponding β-spin unoccupied state is 4.9 eV above the VBM. This state is s-like (state A in Fig. 4) and is, like in the case of the neutral system, a combination of Zr *d* states from the V_2 cavity with the contribution of the bridging Zr atom larger than that of the other Zr centers. The largest contribution comes from the *d* orbitals of the bridging Zr ion, which also extend to the V_1 cavity, although to a smaller degree. The second vacancy state, which is virtual, is located 5.8 eV above the VBM. This state is similar to the state B in Fig. 4 in the neutral system, as it is a combination of Zr *d* states from both vacancies, although the *d* contributions from the V_1 cavity have more weight than contributions coming from the V_2 cavity. The bridging Zr atom states have again a larger contribution than the other states, but not as pronounced as in the previous case. The third vacancy state (state C in Fig. 4) is split 0.3 eV from the CBM. This state is a combination of the $d_{x^2-y^2}$ orbital of the bridging Zr atom with *d* orbitals of the nearest Zr ions in both vacancies. In this case the oxygen contributions are marginal. The fourth vacancy state is split only by 0.1 eV from CBM. In this state (see State D, Fig 4), the d_{z^2} state of the bridging Zr ion mixes with the d^{z^2} orbitals of the Zr ions

nearest to the V_1 cavity. Finally, the resonant state in the conduction band is positioned at 0.3 eV above the CBM. This state (see State E, Fig. 4) is mainly composed of *d* orbitals of Zr atoms surrounding the V_1 vacancy.

The trapped electron modifies the charge distribution of the system with a significant part of the additional negative charge being localized at the bridging Zr atom, which becomes 0.2 e more negative, according to NPA. Some charge, about 0.07-0.1 e, is redistributed between the three NN-Zr atoms and one of the Y atoms of the cluster in the V_2 cavity. The spin population also reflects this distribution, with large spin density on the bridging Zr and smaller amounts on the Zr ions forming the V_2 cavity. The V_1 cavity remains almost unchanged from the neutral state. This result is remarkable, as this charge distribution is very different from that observed for the V^{2+} and V^{+} defects of pure ZrO_2 considered independently, and supports the idea that the spectroscopic features in reduced samples can be related to the presence of Zr^{3+} species [11].

3.1. Spectroscopic properties of divacancy centres

To further assign the nature of defect centres in YSZ one needs to compare their spectroscopic properties to the experimental data. Optical transitions have been calculated using the TDDFT method, and can be classified in four types. These are: band-to-band transitions (Type I), transitions from the valence band to unoccupied vacancy levels (Type II), transitions from occupied vacancy states to conduction band states (Type III), and transitions from occupied vacancy states to resonant localized states created by the vacancy (Type IV). In the neutral system, there are only transitions of types I and II. Optical transitions to the lowest localized state start at 4.23 eV.

In the negatively charged system, Type III optical transitions start at 3.01 eV. Type IV transitions are present at 1.93 eV, 2.24 eV, and 2.67 eV, and have higher oscillator strengths than other transitions due to the localized character of the states involved. These transitions correspond to an electron transfer from one vacancy into the other, and result from the asymmetry of the divacancy complex in our model. The sensitivity of the divacancy states to the local environment around each vacancy may lead to significant modification of these transition energies. Other Type IV transitions are found at 2.80 eV and 3.28 eV, from the middle-gap state to resonant state E inside the conduction band. The energy of this transition is similar to the experimental spectra for the T-center, which show a broad peak with a maximum at 3.3 eV [7]. Type II transitions have an onset of 4.14 eV and small oscillator strength. It's interesting to note that the TD-DFT energies are significantly smaller than the corresponding energy differences between one-electron states, with differences of the order of 0.8-1 eV.

The EPR g-tensor has been calculated for the negatively charged state. The principal values of $g_1 = 1.967$, $g_2 = 1.981$, $g_3 = 1.995$, are similar to the values obtained by other authors [11].

4. Summary and Conclusions

To summarize, we have developed an embedded cluster model for YSZ with doping concentration of 6.3 % per mol. The electronic structure and charge distribution calculated using the B3LYP functional are in agreement with our periodic calculations, demonstrating the applicability of our embedding scheme to ZrO_2. The results predict the formation of different localized levels in the gap of YSZ whose number depends on the charge state of the oxygen divacancy. These states show an asymmetric character related to the different arrangement of Y atoms around each vacancy. Optical transition energies have been calculated for this model using TD-DFT. For the negatively charged state of the divacancy, we obtain a set of transitions at 2.8 eV and 3.3 eV in agreement with experimental data, and a second set of transitions between 1.93 eV and 2.67 eV corresponding to the electron transfer between vacancies. Optical transition energies are larger than their equivalent single particle energy differences, demonstrating the importance of using TD-DFT for accurate predictions. They may be affected by particular arrangements of

dopants near vacancies. The calculated EPR g-tensor values are in agreement with other works. The results support the proposed attribution of the optical absorption peaking at 3.3 eV and related EPR spectra to Zr^{3+} ions in the YSZ matrix, however, they are not fully conclusive. Further extension of this work requires considering other structural arrangements of Y dopant ions, creating structural models corresponding to higher levels of Y doping, comparing their properties with this model, and considering the effect of other dopants, such as Ti, in the matrix of YSZ.

Acknowledgments

DMR is supported by the EPSRC Materials Modelling initiative project GR/S00800/01. The computer time on the HPCx facility was awarded to the Materials Chemistry consortium under EPSRC grant GR/S13422/01 'Materials Chemistry using Teraflop Computing'. The authors are grateful to P. Sushko and J. Gavartin for useful discussions and help in calculations.

References

[1] Subbarao E C 1990 *Ferroelectrics* **102** 267
[2] Taylor D P, Simpson W C, Knutsen K, Henderson M A and Orlando T M 1998 *Appl. Surf. Sci.* **127-129** 101
[3] Cox B 1987 *J. Nuc. Mater.* **148** 332
[4] Orlando R, Pisani C, Roetti C and Stefanovich E 1992 *Phys. Rev. B* **45** 592
[5] Orlando R, Pisani C, Ruiz E and Sautet P 1992 *Surf. Sci.* **275** 482
[6] Bogicevic A and Wolverton C 2003 *Phys. Rev. B* **67** 024106
[7] Orera V M, Merino R I, Chen Y, Cases R and Alonso P J 1990 *Phys. Rev. B* **42** 9782
[8] Azzoni C B and Paleari A 1996 *Phys. Rev. B* **53** 5
[9] Stapper G, Bernasconi M, Nicoloso N and Parrinello M 1999 *Phys. Rev. B* **59** 797
[10] Merino R I, Orera V M, E L E and Kh B S 1995 *Phys. Rev. B* **52** 6150
[11] Pietrucci F, Bernasconi M, di Valentin C, Mauri F and Pickard C J 2006 *Phys. Rev. B* **73** 134112
[12] Sauer J and Sierka M 2000 *J. Comp. Chem.* **21** 1470
[13] Pisani C, Cora F, Nada R and Orlando R 1994 *Comput. Phys. Comm.* **82** 139
[14] Pisani C, Casassa S and Cora F 1994 *Comput. Phys. Comm.* **82** 157
[15] Pisani C and Cora F 1994 *Comput. Phys. Comm.* **82** 168
[16] Pisani C and Cora F 1994 *Comput. Phys. Comm.* **82** 179
[17] Pisani C and Cora F 1994 *Comput. Phys. Comm.* **82** 187
[18] Zhang Y, Lin H and Truhlar D G 2006 *J. Chem. Theory Comput.* **3** 1378
[19] Shluger A L, Kotomin E A and Kantorovich L N 1986 *J. Phys. C: Solid State Phys.* **19** 4183
[20] Zuo J, Pandey R and Kunz A B 1991 *Phys. Rev. B* **44** 7187
[21] Scorza E, Birkenheuer U and Pisani C 1997 *J. Chem. Phys.* **107** 9645
[22] Nasluzov V A, Rivanenkov A B, Gordienko A B, Neyman K N, Birkenheuer U and Rösch N 2001 *J. Chem. Phys.* **115** 8157
[23] Llusar R, Casarrubios M, Barandiarán Z and Seijo L 1996 *J. Chem. Phys.* **105** 5321
[24] Sushko P V, Shluger A L and Catlow C R A 2000 *Surf. Sci.* **450** 153
[25] Carrasco J, Sousa C, Illas F, Sushko P V and Shluger A L 2006 *J. Chem. Phys.* **125** 074710
[26] Sulimov V B, Sushko P V, Edwards A H, Shluger A L and Stoneham A M 2002 *Phys. Rev. B* **66** 024108
[27] Shor A M, Shor E A I, Nasluzov V A, Vayssilov G N and Rösch N 2007 *J. Chem. Theory Comput.* **3** 2290
[28] Smirnov M, Mirgorodsky A and Guinebretiere R 2003 *Phys. Rev. B* **68** 104106
[29] Minervini L, Grimes R W and Sickafus K E 2000 *J. Am. Ceram. Soc.* **83** 1873
[30] Kresse G and Furthmüller J 1996 *Comp. Mat. Sci.* **6** 15
[31] Dovesi R, Saunders V, Roetti C, Orlando R, Zicovich-Wilson C M, Pascale F, Civalleri B, Doll K, Harrison N M, Bush B and D'Arco P L M 2006 *CRYSTAL 2006 User's Manual* (University of Torino)
[32] Towler M D, Allan N L, Harrison N M, Saunders V R, Mackrodt W C and Apra E 1994 *Phys. Rev. B* **50** 5041
[33] Frisch et al M J 2003 *GAUSSIAN 03 Revision C02* (Gaussian Inc.: Wallingford, CT)
[34] Muñoz Ramo D, Gavartin J L, Shluger A L and Bersuker G 2007 *Phys. Rev. B* **75** 205336